Inorganic Chemistry

Article

pubs.acs.org/IC

Coordination Site Disorder in Spinel-Type $LiMnTiO_4$

Denissa T. Murphy,[†] Siegbert Schmid,*[,†] James R. Hester,[‡] Peter E. R. Blanchard,[†,§] and Wojciech Miiller[†,‡]

[†]School of Chemistry, The University of Sydney, Sydney NSW 2006, Australia

[‡]Bragg Institute, Australian Nuclear Science and Technology Organisation, Menai NSW 2234, Australia

Supporting Information

ABSTRACT: $LiMnTiO_4$ was prepared through solid-state syntheses employing different heating and cooling regimes. Synchrotron X-ray and neutron powder diffraction data found quenched $LiMnTiO_4$ to form as single phase disordered spinel (space group $Fd\bar{3}m$), whereas slowly cooled $LiMnTiO_4$ underwent partial phase transition from $Fd\bar{3}m$ to $P4_332$. The phase behavior of quenched and slowly cooled $LiMnTiO_4$ was confirmed through variable-temperature synchrotron X-ray and neutron powder diffraction measurements. The distribution of Li between tetrahedral and octahedral sites was determined from diffraction data. Analysis of the Mn/Ti distribution in addition required Mn and Ti K-edge X-ray absorption near-edge structure spectra. These revealed the presence of Mn^{3+} in primarily octahedral and Ti^{4+} in octahedral and tetrahedral environments, with very slight variations depending on the synthesis conditions. Magnetic measurements indicated the dominance of antiferromagnetic interactions in both the slowly cooled and quenched samples below 4.5 K.

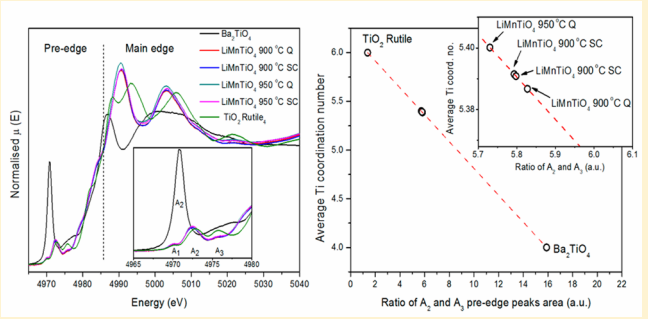

1. INTRODUCTION

Spinel-type lithium metal oxides are attractive cathode materials for rechargeable lithium ion batteries. In particular, $LiMn_2O_4$ was considered a promising cathode material as it is relatively cheaper, environmentally more friendly, and safer to operate than the widely used $LiCoO_2$.[1,2] However, this cathode material suffers structural degradation on cycling due to the presence of Jahn−Teller active Mn^{3+}.[3] Partial substitutions of manganese with other transition metal ions have been studied to improve the electrochemical performance of $LiMn_2O_4$, for example, the spinel $LiNi_{0.5}Mn_{1.5}O_4$ showing improved electrochemical performance at a higher voltage range.[4−6] Cycling behavior of $LiNi_{0.5}Mn_{1.5}O_4$ is still an ongoing problem due to structural instabilities.[7] Doping of $LiMn_2O_4$ with tetravalent titanium was reported to increase the stability of the structure.[8,9] The presence of Ti^{4+} is able to suppress the Jahn−Teller effect of Mn^{3+} resulting in a more stable spinel framework, and therefore, the cycling ability is significantly improved. In addition, a recent study on nanophase $LiMnTiO_4$ showed that capacities up to 290 mA h g^{-1} are achievable, rendering the material a very attractive electrode material indeed.[10]

The structure of $LiMnTiO_4$ was first analyzed as part of a study into property changes upon the substitution of ruthenium with titanium in the $Li_{1-y}MnRu_{1-x}Ti_xO_4$ system.[11] $LiMnTiO_4$ was reported as a disordered cubic spinel (space group $Fd\bar{3}m$), with a cation distribution of $Li_{0.75}Ti_{0.25}[Li_{0.25}Mn_{1.00}Ti_{0.75}]O_4$ (square brackets denote the octahedral site). It was also noted, however, that it was not possible to distinguish between manganese and titanium on the tetrahedral and octahedral sites due to the small differences in their X-ray scattering factors.

Since that study there has been an ongoing debate on the coordination site disorder and the Mn oxidation states in $LiMnTiO_4$. For the normal spinel $LiMn_2O_4$ the lithium cations occupy the tetrahedral sites, and the manganese cations occupy the octahedral sites. For $LiMnTiO_4$ it was estimated from X-ray diffraction (XRD) data that ∼35% of Li^+ on the tetrahedral sites were replaced by Ti^{4+}. In addition, the oxidation states of manganese and titanium were confirmed by electron energy loss spectroscopy (EELS) to be Mn^{3+} and Ti^{4+}.[12] However, the distribution of these metal ions could not be determined accurately due to the low energy resolution of the spectra. Thus, the substitution of manganese ions with titanium ions results in mixed cation occupancies on both tetrahedral and octahedral sites, that is, Mn^{3+}, Li^+, and Ti^{4+} on the octahedral sites and the remaining Li^+ and Ti^{4+} on the tetrahedral sites.[12]

On the basis of bond valence sum (BVS) calculations for models refined against XRD data, it was proposed that the tetrahedral sites in $LiMnTiO_4$ were partially occupied by Mn^{2+} instead of Ti^{4+}.[13−15] As a consequence the octahedral sites were partially occupied by Mn^{4+}, to compensate for the presence of Mn^{2+}. These results prompted a more comprehensive study of the structure of $LiMnTiO_4$, using a combination of X-ray and neutron powder diffraction, thermogravimetric analysis (TGA), and magnetic measurements.[16] It was proposed that different

Received: November 28, 2014
Published: May 5, 2015

DOI: 10.1021/ic502747p
Inorg. Chem. 2015, 54, 4636−4643

sintering temperatures and cooling regimes had an effect on the phase behavior of $LiMnTiO_4$ and that single-phase $LiMnTiO_4$ (space group $Fd\bar{3}m$) with the metal ion ordering established previously[17] formed upon slowly cooling from the synthesis temperature, while $LiMnTiO_4$ (space group $P4_332$) was found alongside the main $Fd\bar{3}m$ phase upon quenching (Figure 1).

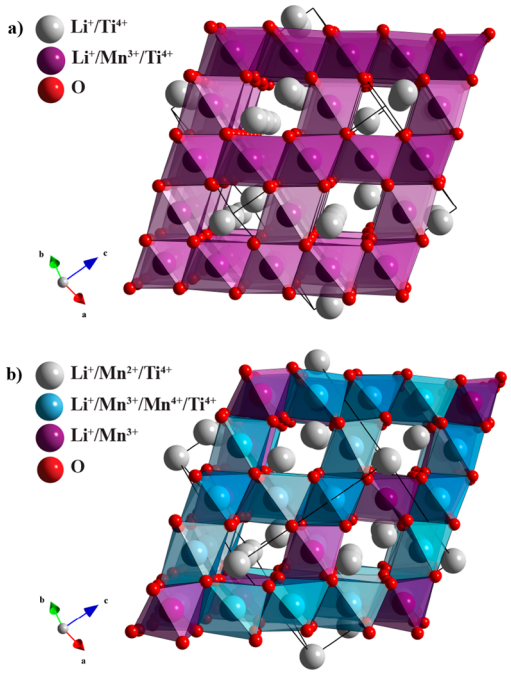

Figure 1. Polyhedral representation of (a) spinel-type $LiMnTiO_4$ (space group $Fd\bar{3}m$) and (b) spinel-type $LiMnTiO_4$ (space group $P4_332$) with the two crystallographically independent octahedral sites represented by the differently colored polyhedra.

The transition from $Fd\bar{3}m$ spinel to $P4_332$ spinel results in two crystallographically independent octahedral sites in the structure. The $P4_332$ spinel phase was found to accommodate Li^+, Mn^{2+}, and Ti^{4+} on the tetrahedral sites, Mn^{4+}, Mn^{3+}, and Li^+ on the 12*d* octahedral sites, and the remaining Mn^{4+}, Mn^{3+}, Li^+, and Ti^{4+} on the 4*b* octahedral sites (see Figure 1).[18]

We first synthesized $LiMnTiO_4$ following the reported procedure[19] but found that slowly cooled $LiMnTiO_4$ formed two phases, whereas on quenching only one phase was formed. Given these contradicting results, further investigations of the temperature dependent phase behavior and associated metal ion ordering for $LiMnTiO_4$ were deemed necessary for a better understanding of this electrode material. It is quite unusual for an important compound to have unresolved metal ion ordering after such a long time, but this is principally due to the difficulty of differentiating between manganese and titanium, owing to their relatively similar X-ray scattering factors as well as neutron scattering lengths. Interestingly, this fact has rarely been mentioned in previous investigations of this material.

In this paper, we report the effects of different thermal treatments, in particular, the cooling regime employed during the synthesis, on the phase behavior and metal ion ordering of $LiMnTiO_4$, with the main emphasis on the single phase $Fd\bar{3}m$ spinel. These results are based on a combination of synchrotron X-ray powder diffraction (SXRD), neutron powder diffraction (NPD), magnetic measurements, and X-ray absorption near edge structure (XANES) spectroscopy. For a better understanding of the influence of different heating and cooling regimes, variable-temperature SXRD and NPD investigations were carried out as well.

2. EXPERIMENTAL SECTION

$LiMnTiO_4$ samples were prepared by the solid-state method. Stoichiometric ratios of Li_2CO_3 (predried at 120 °C, Merck, 99%), $MnCO_3$ (Sigma-Aldrich, 99.99%), and TiO_2 (Aithaca, 99.99%) were ground in a small amount of acetone using an agate mortar and pestle (ball mill for large samples) until dry, then transferred to alumina crucibles and fired in air at 500 °C for 12 h. The calcined samples were reground with acetone until dry and pressed into pellets using a uniaxial pellet press at 8 tons of pressure (large samples were pressed into rods using a hydrostatic press at 500 MPa). Samples were further sintered in air at 900 or 950 °C, followed by either quenching in liquid nitrogen or slowly cooling in air.

TGA measurements were performed on quenched and slowly cooled $LiMnTiO_4$ samples using a TA Instruments Hi-Res TGA 2950 Thermogravimetric Analyzer. Experiments were performed in air, with a flow rate of 20 mL/min during data collection. Samples were heated from 25 to 900 °C, held at 900 °C for 30 min, and then cooled to room temperature. The heating and cooling rates were set at 5 °C/min.

Synchrotron X-ray powder diffraction data were collected at the powder diffraction beamline (10-BM) of the Australian Synchrotron. Using LaB_6 (NIST standard 660a) the wavelength was accurately determined to be 0.826 57(1) Å. Samples for collection at room temperature and high temperature were packed into 0.3 mm diameter glass and quartz capillaries, respectively, and sealed in air. Data were collected in the range of $2° < 2\theta < 82.5°$. The data were collected over two frames shifted by 0.5° to cover the gaps in the modular detector approximately every 5°. Prior to analysis, the data obtained from the two detector positions were spliced, that is, data from each position were normalized against a common reflection, then the gaps in frame one were filled with data from frame two resulting in a complete data set over the 2θ range of 2−82.5°. High-temperature data were collected using a hot-air blower rated to ±1 °C.

NPD data were collected using the ECHIDNA high-resolution powder diffractometer at the OPAL reactor, Australian Nuclear Science and Technology Organisation (ANSTO), using a wavelength of 1.622 Å between $5° < 2\theta < 165°$ with a step size of 0.05° over a period of 3 h. Samples were placed into 9 mm diameter vanadium cans for room-temperature collections in a vacuum furnace. High-temperature data were collected using an air furnace and a 9 mm diameter alumina sample holder. The structural characterization of the materials was performed through Rietveld refinement[20] using Jana2006[21] for both the X-ray and neutron data.

Magnetisation and magnetic susceptibility measurements were performed using a P525 Vibrating Sample Magnetometer (VSM) option of a Quantum Design Physical Property Measurement System (PPMS) in the range of $2\ K \leq T \leq 390\ K$ in a field of 1 T. Approximately 35 mg of the polycrystalline materials were packed into polymer capsules and secured using Kapton tape.

Manganese and titanium K-edge XANES spectra were collected using the Australian National Beamline Facility (ANBF), BL20B, Photon Factory, Tsukuba, Japan. Homogeneous mixtures of the samples and boron nitride (BN) were packed onto sample holders with approximate diameter of 0.2 cm and covered with Kapton tape. Energy steps of 0.25 eV were employed with counting time of 2 s per step. Energy calibration was performed through simultaneous absorption measurements using Mn and Ti metal foils, respectively. Analysis of XANES spectra was performed using the Athena program within the IFEFFIT[22] software package. Pre-edge area calculations were performed using the CasaXPS software package.[23]

3. RESULTS AND DISCUSSION

The SXRD patterns of quenched and slowly cooled $LiMnTiO_4$ sintered at 900 and 950 °C, respectively, are shown in Figure 2. Both quenched $LiMnTiO_4$ samples were modeled as cubic

DOI: 10.1021/ic502747p
Inorg. Chem. 2015, 54, 4636−4643

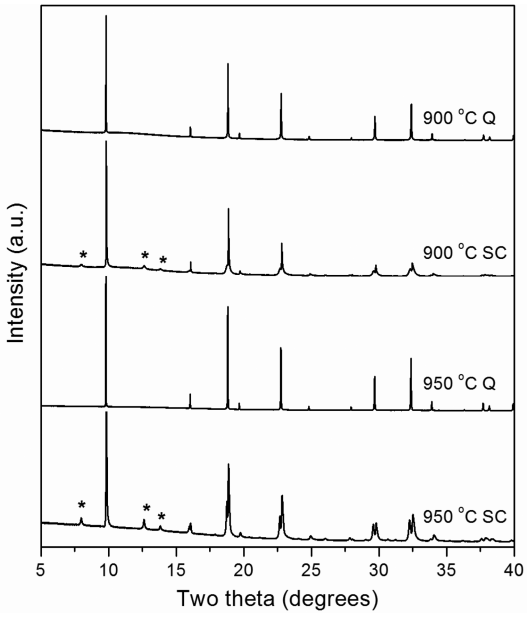

Figure 2. SXRD patterns of $LiMnTiO_4$ synthesized at 900 and 950 °C. Q and SC denote quenched and slowly cooled samples, respectively. The asterisks indicate the low-angle reflections characteristic of the $P4_332$ phase.

spinel (space group $Fd\bar{3}m$). Additional reflections at low 2θ were present alongside the $Fd\bar{3}m$ phase in the patterns of both slowly cooled $LiMnTiO_4$ samples (see asterisks in Figure 2). These reflections were indexed as the 101, 102, and 112 peaks, which are additional for the $P4_332$ phase.

NPD data of quenched $LiMnTiO_4$ were entirely consistent with those observations. Both samples, quenched from 900 and 950 °C, respectively, were refined in the cubic $Fd\bar{3}m$ space group. Comparison of the neutron diffraction data revealed virtually identical patterns apart from the presence of two small impurity peaks in the sample quenched from 950 °C.

TGA was performed for both quenched and slowly cooled samples of $LiMnTiO_4$. For the sample slowly cooled from 900 °C a very small mass gain (<0.1%) was observed on heating in air to 700 °C. On further heating to 900 °C, ~1.4% of the mass was lost, corresponding to 0.15 O per formula unit. This indicates that the slowly cooled sample is fully oxidized and contains no oxygen vacancies at RT. In contrast, the sample quenched from 900 °C gained a small amount of mass (0.7%, ~0.08 O per formula unit) when heated to 700 °C. On further heating to 900 °C a similar amount of mass was lost as for the slowly cooled sample. It would therefore appear that $LiMnTiO_4$ at the synthesis temperature loses a small amount of oxygen, which it is able to regain when slowly cooled, but not on quenching.

As indicated in the introduction the refinement of the $LiMnTiO_4$ spinel structure, which has only one refinable positional parameter in space group $Fd\bar{3}m$, is complicated by the very similar X-ray scattering factors and very similar neutron scattering lengths for both Ti and Mn (22 vs 25 electrons and b_{coh} of −3.37 vs −3.75, respectively). In addition the low X-ray scattering factor for Li means that X-ray diffraction data on their own are not very useful for the determination of the metal ordering in this structure. Consequently, a combined refinement against neutron and X-ray powder diffraction data was performed. The metal ordering as determined previously from XPS and EELS data was used as a starting point.[12,17] The refinement program Jana2006[21] allowed for constraint refinement of two atoms on one crystallographic site but not three. Consequently, we started varying Li and Ti occupancies on the tetrahedral and octahedral sites, keeping the overall sum constant. The occupancy of Mn on the octahedral site was kept as 50%. To test the robustness of the results the occupancies were moved far away from the expected values, but the same result was observed in all cases, that is, Ti ≈ 32%, Li ≈ 68% on the tetrahedral site and Ti ≈ 34%, Li ≈ 16% on the octahedral site (note the multiplicity of the octahedral site is twice that of the tetrahedral site). The atomic displacement parameters (ADPs) of Li and Ti for each site were constrained to be identical.

Once the distribution of Li between the tetrahedral and octahedral sites was established, it was possible to consider the distribution of Ti and Mn between these sites. While the refinement of the Li distribution between the sites was fairly robust owing to the large difference between Li and Ti/Mn scattering factors/lengths, the refinement of the exact Ti/Mn distribution between the sites was less stable. The refinements often resulted in unrealistic occupancy values on both the tetrahedral and octahedral sites. The most stable refinement was achieved with 30.0% Ti and 2.5% Mn on the tetrahedral sites (this value is quite compatible with the amount of oxygen vacancies determined from TGA data). Note, however, that if the occupancies of Ti and Mn are interchanged while keeping the ADPs constant, the resulting R values do not change significantly. The refined NPD profile is shown in Figure 3, and selected refinement parameters and crystallographic data for the combined X-ray and neutron refinement are listed in Table 1.

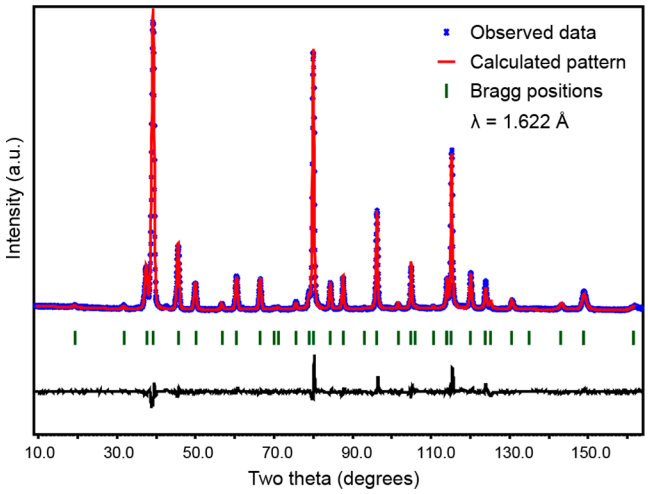

Figure 3. NPD pattern of $LiMnTiO_4$ quenched from 900 °C. The small peak at 43° 2Θ is due to an unidentified impurity (see Supporting Information, Figure S1).

Utilizing the bond lengths resulting from the combined refinement of quenched $LiMnTiO_4$, BVS values for the metal ions on the different cation sites were calculated.[24] For the tetrahedral 8*a* sites the BVS values for Li^+, Ti^{4+}, and Mn^{2+} are 0.933, 2.397, and 2.241, respectively. For the octahedral 16*d* sites, the BVS for Li^+, Ti^{4+}, Mn^{3+}, and Mn^{4+} are 1.450, 3.723, 3.209, and 3.148, respectively. While the BVS values for the tetrahedral site might indicate the suitability of the site for Mn^{2+}, the octahedral site is far from ideal for Mn^{4+}, which is required by charge balance once the small amount of oxygen

DOI: 10.1021/ic502747p
Inorg. Chem. 2015, 54, 4636−4643

Table 1. Selected Refinement Parameters and Crystallographic Data for Quenched $LiMnTiO_4$ from Combined SXRD and NPD Refinement

parameter	$LiMnTiO_4$	
space group	$Fd\bar{3}m$	
a (Å)	8.3808(15)	
V (Å^3)	588.66(18)	
R_B (%)	3.19	
R_{wp} (%)	4.34	
tetrahedral sites 8*a*:	$x = y = z$	occupancy
Li^+	0.125	0.675(5)
Ti^{4+}	0.125	0.300(5)
Mn^{2+}	0.125	0.025(5)
octahedral sites 16*d*:	$x = y = z$	occupancy
Li^+	0.5	0.163(3)
Ti^{4+}	0.5	0.350(3)
$Mn^{3+/4+}$	0.5	0.488(3)
oxygen sites 32*a*:	$x = y = z$	Occupancy
O^{2-}	0.2630(3)	0.98

vacancies, < 2% as determined by TGA measurements, is exhausted. Note that BVS values calculated for mixed sites must be interpreted with care, since they necessarily represent an average environment that may not be adopted by any of the involved ions. The analysis of BVS is generally a very useful empirical tool, but on this occasion it is inconclusive.

Variable-temperature SXRD measurements were performed for $LiMnTiO_4$ quenched from 900 °C to further investigate its phase behavior and to ascertain its high-temperature structure. Synchrotron XRD patterns were collected between 30 and 950 °C with a heating rate of 5 °C/min between data collections (Figure 4a). Upon heating, unit cell expansion was observed, but there was no change of the $Fd\bar{3}m$ symmetry, confirming that the high-temperature structure of $LiMnTiO_4$ is the cubic $Fd\bar{3}m$ spinel. At 850 °C additional reflections appeared, which are likely due to a side reaction of Li with the quartz capillary. These reflections became more pronounced at 900 and 950 °C. On cooling another impurity peak started to appear from 875 °C.

After the temperature reached 950 °C, quenched $LiMnTiO_4$ was slowly cooled at a rate of 10 °C/min, and SXRD patterns were collected. A partial phase transition from the $Fd\bar{3}m$ cubic spinel to the $P4_332$ cubic spinel occurred between 575 and 650 °C indicated by the appearance of the 101, 102, and 112 reflections characteristic of $P4_332$ symmetry (Figure 4b). This is a consequence of partial ordering of the cations, which resulted in the formation of the more highly ordered, lower symmetry $P4_332$ phase. Despite the small impurities formed during the investigation, this study of the thermal behavior of $LiMnTiO_4$ is consistent with a single phase appearing on quenching and a two-phase mixture appearing on slowly cooling from the synthesis temperature. The cell dimension of the phase on completion of the variable-temperature experiment was 8.4305 (15) Å, that is, there was a significant increase, most likely due to the increased oxygen content in the sample.

Variable-temperature NPD data were collected at 30, 427, 577, and 827 °C with a heating rate of 5 °C/min between collections. An alumina sample holder was used to allow the data collection to be performed in air, to emulate the synthesis

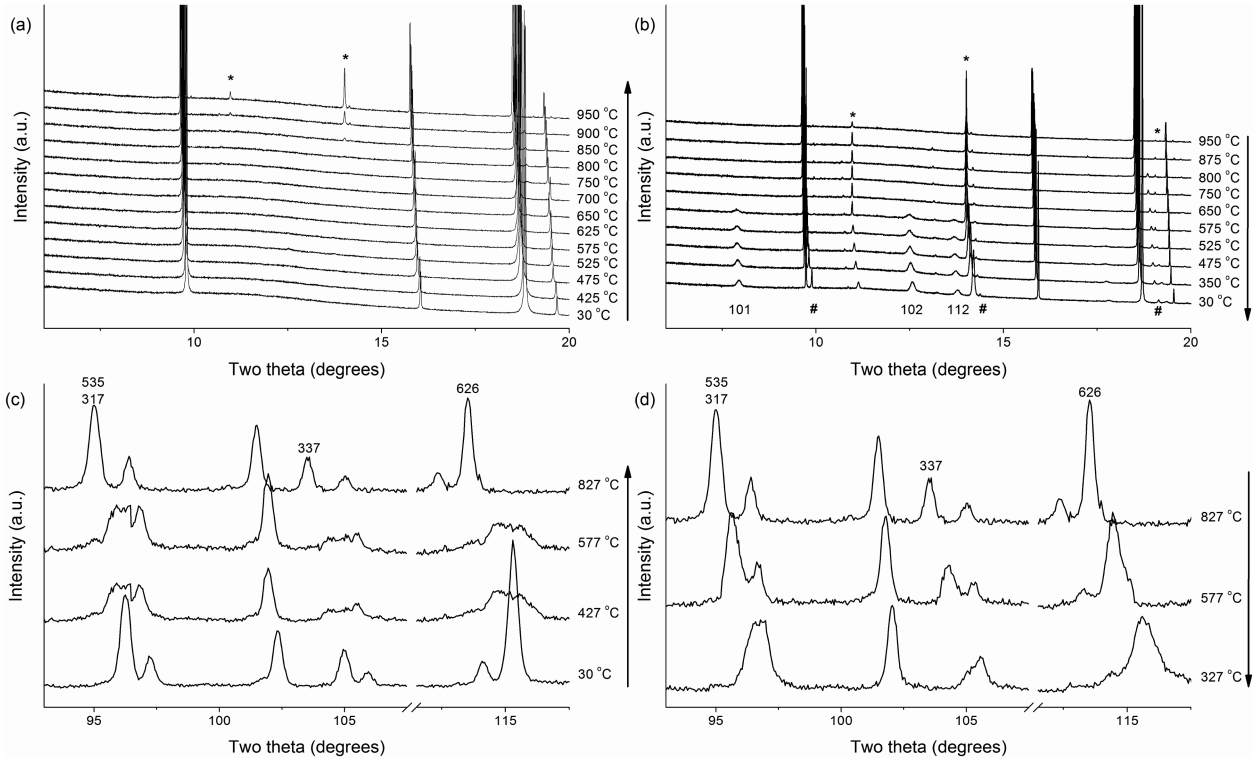

Figure 4. Variable-temperature SXRD (a, b) and NPD (c, d) patterns of $LiMnTiO_4$ quenched from 900 °C on heating (a, c, respectively) and cooling (b, d, respectively). (b) The 101, 102, and 112 reflections, corresponding to the $P4_332$ phase, were seen on cooling only. The asterisks denote an impurity phase formed though reaction with the capillary. The hashes indicate a second impurity phase formed upon cooling. (c, d) Broadening of the 535, 317, 337, and 626 reflections in the NPD patterns indicates the partial formation of the $P4_332$ phase. The remaining unindexed peaks stem from the alumina sample holder and furnace utilized for the NPD experiment.

DOI: 10.1021/ic502747p
Inorg. Chem. 2015, 54, 4636−4643

conditions. Reflections contributed by the alumina sample holder and the furnace were of significant intensity, and some of the most intense reflections overlapped with the $LiMnTiO_4$ phase, complicating the refinement process. The room-temperature diffraction pattern was refined as the $Fd\bar{3}m$ phase, in agreement with the SXRD data. As the sample was heated there was broadening of many $Fd\bar{3}m$ reflections, indicating the onset of the $P4_332$ phase. In Figure 4c this is shown for the 535, 317, 337, and 626 reflections. At 827 °C, the peak broadening diminished, and the pattern resembled the room-temperature data, confirming that at high temperature only the $Fd\bar{3}m$ phase was present. Cooling the sample to 327 °C again resulted in broadening of the $Fd\bar{3}m$ phase peaks (Figure 4d). These observations are fully consistent with the syntheses results. Importantly only a single phase ($Fd\bar{3}m$) exists at high temperature, and a second phase ($P4_332$) formed alongside the main phase as the sample was slowly cooled.

Investigation of slowly cooled $LiMnTiO_4$ was performed as well. Slow cooling of $LiMnTiO_4$ was performed at the natural cooling rate of the furnace, which was established to be 6 °C/min for the first 15 min of cooling, but decreased to 3 °C/min from then on. Room-temperature SXRD patterns were collected for slowly cooled $LiMnTiO_4$ sintered at 900 and 950 °C. As shown in Figure 2, both slowly cooled $LiMnTiO_4$ samples show the reflections characteristic of the $P4_332$ phase in addition to those of the $Fd\bar{3}m$ phase. Attempts to transform the sample completely to the $P4_332$ phase were unsuccessful.

To confirm the two-phase nature of $LiMnTiO_4$ slowly cooled from 950 °C a room-temperature NPD pattern was collected (Figure 5). The $Fd\bar{3}m$ model of the quenched sample (see above) served as a starting point for the refinement. The $Fd\bar{3}m$ phase was refined first to attain a stable refinement. The occupancies and the ADPs of this phase were then fixed before the $P4_332$ structure was refined. The model of the $P4_332$ phase was refined after imposing the cation distribution previously reported for this phase as a starting point.[16] All cation sites have mixed occupancy with Li^+, Ti^{4+}, and Mn^{2+} on the tetrahedral site and Li^+, Ti^{4+}, Mn^{3+}, and Mn^{4+} ions occupying the octahedral sites. It was determined that ~35% of the $P4_332$ phase is present alongside the $Fd\bar{3}m$ phase in slowly cooled $LiMnTiO_4$. The refinement parameters and crystallographic data are given in Table 2.

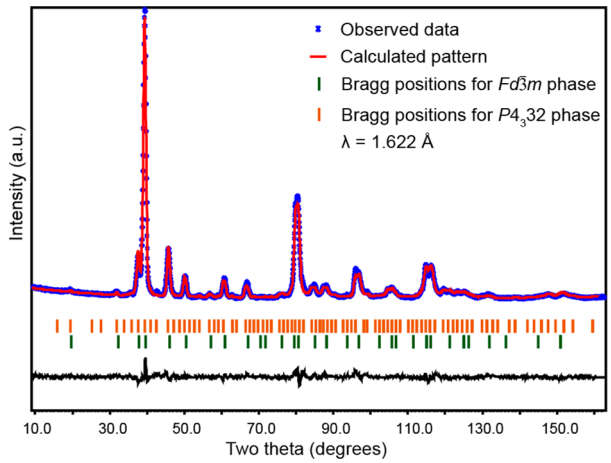

Figure 5. NPD pattern of $LiMnTiO_4$ slowly cooled from 950 °C. The peak at 43° 2Θ is due to an unidentified impurity.

Table 2. Refinement Parameters and Crystallographic Data for $LiMnTiO_4$ Slowly Cooled from 900 °C (from NPD data)

parameter	$LiMnTiO_4$			
space group	$Fd\bar{3}m$		$P4_332$	
a (Å)	8.3408(6)		8.4077(6)	
V (Å^3)	580.25(7)		594.33(7)	
R_B (%)	5.17		9.49	
R_{wp} (%)	8.53		10.89	
phase fraction	0.650(17)		0.350(12)	
tetrahedral:	8*a*		8*c*	
	$x = y = z$	occ.	$x = y = z$	occ.
Li^+	0.125	0.754(12)	0.0129(17)	0.629(15)
Ti^{4+}	0.125	0.245(12)	0.0129(17)	0.263(15)
Mn^{2+}			0.0129(17)	0.106(15)
octahedral:	16*d*		4*b*	
	$x = y = z$	occ.	$x = y = z$	occ.
Li^+	0.5	0.123(6)	0.625	0.140(3)
Ti^{4+}	0.5	0.377(6)		
*$Mn^{3+/4+}$	0.5	0.5	0.625	0.870(3)
octahedral:			12*d*	
				occ.
Li^+			x = 0.125,	0.200(10)
Ti^{4+}			y = 0.374(13)	0.491(10)
$Mn^{3+/4+}$			z = 0.876(13)	0.308(10)
oxygen sites:	32*a*		8*c*	
O^{2-}	$x = y = z$	occ.	$x = y = z$	occ.
	0.2624(1)	1	0.388(6)	1
			24*e*	
			x = 0.122(6),	occ.
			y = 0.0999(4), z = 0.384(6)	1

* Mn^{4+} only for $P4_332$ phase

Variable-temperature SXRD studies were performed on $LiMnTiO_4$ slowly cooled from 900 °C to investigate the thermal behavior up to the synthesis temperature. As the sample was heated a phase transition from the $P4_332$ cubic spinel to the $Fd\bar{3}m$ cubic spinel occurred between 425 and 475 °C. There was no further change to this phase as the temperature was increased. An impurity phase forming above 800 °C is similar to that observed during the variable-temperature measurements of quenched $LiMnTiO_4$. The cell dimension on return to room temperature had also slightly increased to 8.4412 (14) Å, that is, to almost the same value as the quenched sample after the variable-temperature experiment.

In summary, synthesis, phase determination, structural characterization, and variable-temperature studies of quenched and slowly cooled $LiMnTiO_4$ have yielded results exactly opposite to those previously reported.[16]

Magnetic measurements of $LiMnTiO_4$ allow the determination of effective moments, which are directly related to the oxidation states of the magnetic ions. In Figure 6, the inverse magnetic susceptibilities, $1/\chi$, versus temperature are plotted for $LiMnTiO_4$ quenched or slowly cooled from 900 °C. Above 125 and 175 K, for the quenched and slowly cooled samples, respectively, the linear region can be described using the Curie–Weiss law. The negative values for the Curie–Weiss temperature of −178 and −127 K for slowly cooled and quenched $LiMnTiO_4$, respectively, suggest the dominance of antiferromagnetic interactions. The magnetic moment of $LiMnTiO_4$ was normalized with respect to manganese, as

DOI: 10.1021/ic502747p
Inorg. Chem. 2015, 54, 4636−4643

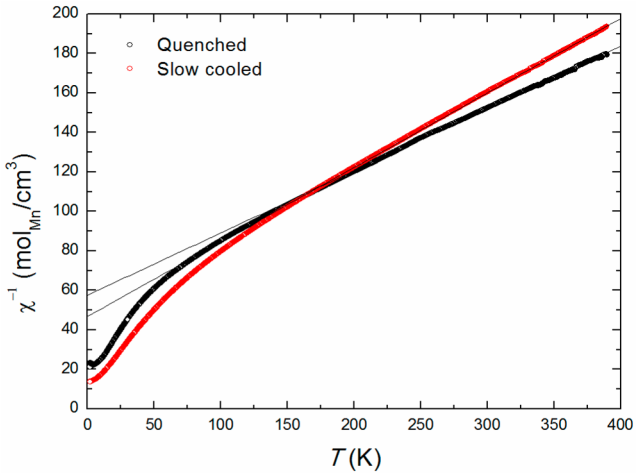

Figure 6. Temperature dependence of the inverse magnetic susceptibility for $LiMnTiO_4$ slowly cooled and quenched from 900 °C measured at B = 1 T.

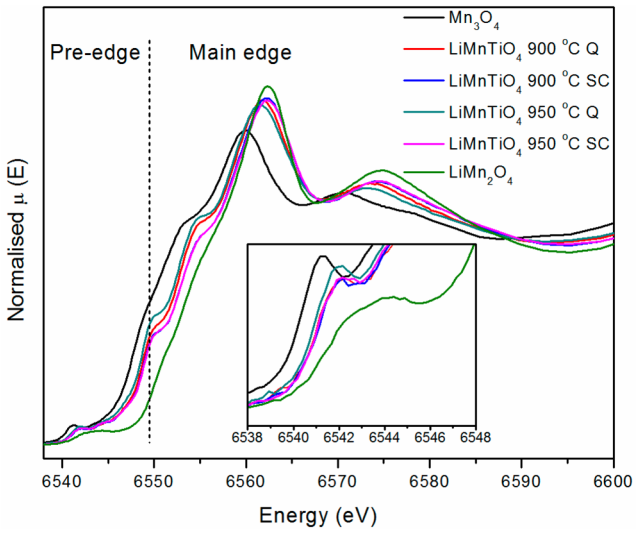

Figure 7. Normalized Mn K-edge spectra of Mn standards and $LiMnTiO_4$ quenched and slowly cooled from 900 or 950 °C. Q and SC denote quenched and slowly cooled samples, respectively.

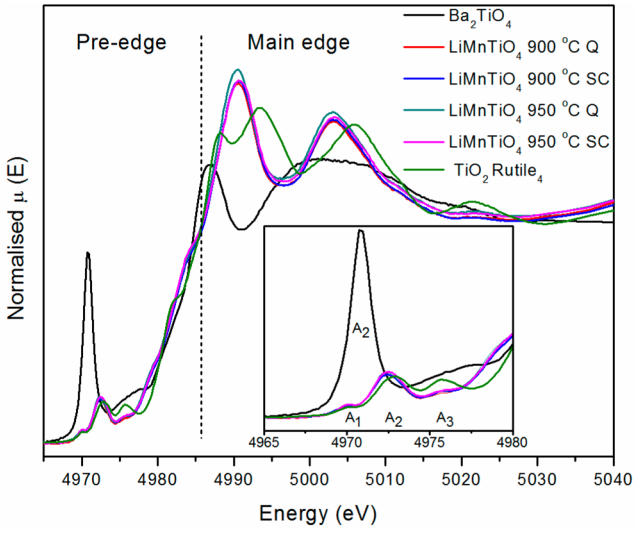

Figure 8. Normalized Ti K-edge spectra of Ti standards and $LiMnTiO_4$ quenched and slowly cooled from 900 °C. Q and SC denote quenched and slowly cooled samples, respectively. (inset) Highlight of the pre-edge peaks.

manganese is the only metal in the structure with unpaired electrons. The effective moment μ_{eff} = 4.62 μ_B/Mn for quenched $LiMnTiO_4$ is in good agreement with the reported effective moment of 4.54 μ_B/Mn for slowly cooled $LiMnTiO_4$.[16] The value μ_{eff} = 5.03 μ_B/Mn for slowly cooled $LiMnTiO_4$ is also in a good agreement with the effective moment for Mn^{3+} and with the effective moment of 5.0 μ_B/Mn for quenched $LiMnTiO_4$ reported earlier.[16] The higher effective moment observed for the slowly cooled sample might suggest release of some structural or magnetic frustration during slow cooling. This latter point is apparent in the higher absolute value of the characteristic Curie–Weiss temperature than for the quenched sample.

Mn and Ti K-edge XANES spectra were collected for $LiMnTiO_4$ quenched and slowly cooled from 900 and 950 °C to further confirm the oxidation states and coordination environments of the transition metal ions. The oxidation states of manganese and titanium in $LiMnTiO_4$ can be established through matching the positions of the absorption edges with those of well-characterized oxide standards. In addition the coordination chemistry can be determined through comparison of the pre-edge features in $LiMnTiO_4$ spectra with compounds containing manganese and titanium ions located in either or both of the tetrahedral and octahedral sites.[25,26] Comparison of the Mn K-edge spectra for quenched and slowly cooled $LiMnTiO_4$ shows that all samples have similar absorption-edge energies (Figure 7). Well-resolved edge features were seen in Ti K-edge spectra (Figure 8) of the quenched and slowly cooled samples. No shift of the absorption energies was observed, consistent with a single oxidation state for titanium.

The Mn K-edge spectra of $LiMnTiO_4$ were compared to several standards containing combinations of Mn^{2+}, Mn^{3+}, and Mn^{4+} in different coordination environments (Figure 7). For manganese oxides, the K-edge absorption edge energy is directly proportional to the manganese oxidation state, that is, the energy generally increases as the oxidation state increases.[25,27] There are two important features of the Mn K-edge: the pre-edge and the main edge. The main edge features arise from a dipole allowed transition of a 1s electron into manganese 4p states hybridized with oxygen bonding overlap and delocalized states.[27,28] The pre-edge feature is seen for a majority of 3d transition-metal K-edges and arises from the dipole-forbidden 1s to 3d transition.

Comparison of the samples' spectra with the standards shows that the absorption energies of quenched and slowly cooled $LiMnTiO_4$ were in between that of Mn_3O_4 ($Mn^{2+/3+}$) and the spinel $LiMn_2O_4$ ($Mn^{3+/4+}$), albeit slightly higher for the slowly cooled samples than the quenched samples, consistent with the TGA results indicating a slight oxygen deficiency in the quenched samples. Comparison of the pre-edge features with those of Mn_3O_4, which has Mn^{2+} on the tetrahedral sites, suggests that the presence of tetrahedral Mn^{2+} in $LiMnTiO_4$ quenched from 950 °C is possible, while for the other samples it is unlikely. This is indicative of the presence of octahedrally coordinated Mn^{3+} in the sample quenched from 900 °C and entirely consistent with the results of an EELS investigation.[12]

The Ti K-edge spectra of $LiMnTiO_4$ samples and standards with Ti in tetrahedral and octahedral coordination are shown in

DOI: 10.1021/ic502747p
Inorg. Chem. 2015, 54, 4636–4643

Figure 8. Comparison of the Ti K-edge absorption-edge energies of the $LiMnTiO_4$ samples with the standards confirms the presence of Ti^{4+}. Careful analysis of the pre-edge features provides information on the coordination number of Ti in $LiMnTiO_4$. The Ti K-edge pre-edge features are also highlighted in Figure 9. Both quenched and slowly cooled

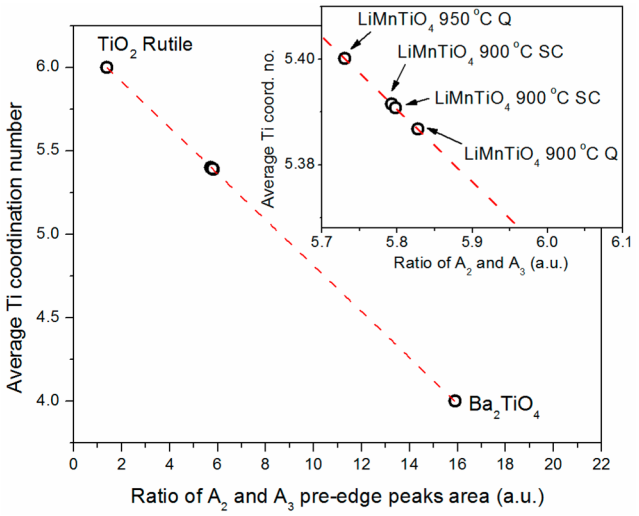

Figure 9. Plot of average coordination number of Ti vs the ratio of A_2 and A_3 pre-edge peak areas for $LiMnTiO_4$ and standards. Inset: Magnified region showing positions of $LiMnTiO_4$. Q and SC denote quenched and slowly cooled samples, respectively.

$LiMnTiO_4$ had three distinct peaks (labeled A_1-A_3), with peak A_1 commonly attributed to the presence of octahedral Ti^{4+}. In octahedral systems, feature A_1 is a dipole-forbidden 1s−3d t_{2g} transition.[29−31] Feature A_2 corresponds to the transition of a 1s electron into hybridized Ti 3d/4p states with e_g symmetry. The intensity of this feature is greatly influenced by the coordination number of the Ti^{4+} cation. In general, this feature increases in intensity as the coordination number decreases from 6 to 4 due to an increase in Ti 3d/4p hybridization. Feature A_3, which corresponds to transitions of a 1s electron into the 3d states of neighboring Ti^{4+} cations, should decrease in intensity with decreasing coordination number.

Fitting the pre-edge peaks using Lorentzian functions to extract the area of the peaks has been utilized previously to correlate the change of peak intensities with the average coordination numbers.[29−31] The change of these peak intensities can be used to determine the amount of Ti^{4+} present on the tetrahedral sites. The peak areas of the pre-edge features for Ba_2TiO_4, TiO_2, and $LiMnTiO_4$ (quenched and slowly cooled) were calculated. The ratios of the A_2 and A_3 peak areas of Ba_2TiO_4 and TiO_2 (the A_1 peak corresponds to the quadruple s→d transition and is not relevant in this calculation) were then plotted against the coordination number in these compounds (Figure 9). The average coordination numbers for the $LiMnTiO_4$ samples were obtained from the line of best fit. They are 5.39 and 5.40 for $LiMnTiO_4$ quenched from 900 and 950 °C, respectively, and 5.39 for both slowly cooled samples. These values suggest the presence of 30% of Ti^{4+} on the tetrahedral sites for all investigated samples. This value is consistent with the amount of Ti^{4+} in tetrahedral coordination from the structural refinements. In addition, this is also in line with results from X-ray photoelectron spectroscopy, showing for the surface area that 34% of Ti^{4+} replaces Li^+ on the tetrahedral sites.[17]

4. CONCLUSION

The cubic spinel $LiMnTiO_4$ was synthesized employing different heating and cooling regimes and was structurally characterized. While our procedures followed previously published ones, we obtained exactly opposite results.[16] Most importantly, $LiMnTiO_4$ formed a single-phase cubic spinel ($Fd\bar{3}m$) on quenching, while slowly cooled $LiMnTiO_4$ consisted of cubic spinel phases with $Fd\bar{3}m$ (65%) and $P4_332$ (35%) symmetries.

The plausibility of these results was verified through variable-temperature X-ray and neutron diffraction experiments, which showed that at the synthesis temperatures only the single-phase $Fd\bar{3}m$ spinel existed. Our synthesis is consistent with this finding, since it would not be expected that a second phase forms on quenching. Instead, partial phase transition from the $Fd\bar{3}m$ to $P4_332$ symmetry occurred upon slowly cooling during the variable-temperature SXRD measurement, again consistent with our synthesis results. On heating, the reverse phase transition from $P4_332$ to $Fd\bar{3}m$ was observed between 425 and 475 °C in the variable-temperature SXRD measurement for slowly cooled $LiMnTiO_4$.

Determination of metal ordering is not straightforward for LiMnTiO4, since Mn and Ti have very similar X-ray scattering factors and neutron scattering lengths (and with almost identical relative differences). While the distribution of Li between the tetrahedral and octahedral sites could be established from the combined refinement against X-ray and neutron diffraction data, the distribution of Mn and Ti between those sites was more difficult to analyze. The most stable refinement for $LiMnTiO_4$ quenched from 900 °C led to mixed occupancies of 67.5:30.0:2.5 for Li/Ti/Mn on the tetrahedral sites and 16.3:35.0:48.8 for Li/Ti/Mn on the octahedral sites.

Quenched and slowly cooled $LiMnTiO_4$ had negative Curie−Weiss temperatures suggesting the predominantly antiferromagnetic interactions in the systems below 4.5 K. The effective moments of 4.62 μ_B/Mn and 5.03 μ_B/Mn for the quenched and slowly cooled samples, respectively, correspond to the presence of mostly Mn^{3+}.

Comparison of Mn and Ti K-edge XANES spectra of quenched and slowly cooled $LiMnTiO_4$ with well-characterized manganese and titanium standards revealed the presence of Ti^{4+} on tetrahedral (~30%) and octahedral sites (~70%) and predominantly octahedrally coordinated Mn^{3+} for the sample quenched from 900 °C. The slowly cooled sample and those synthesized at 950 °C showed slight differences (including the possible presence of tetrahedral Mn^{2+} for the sample quenched from 950 °C).

We have established for the first time a comprehensive analysis of the metal ion ordering and oxidation states of $LiMnTiO_4$. The combination of structural determination, property measurements, and spectroscopy provided conclusive information for the complex metal ion ordering best represented by $Li_{0.675}Mn_{0.025}Ti_{0.300}[Li_{0.163}Mn_{0.488}Ti_{0.350}]O_4$. This material appears to be very sensitive to different thermal treatments imposed during the synthesis. This sensitivity may account for some of the very different results previously reported.

DOI: 10.1021/ic502747p
Inorg. Chem. 2015, 54, 4636−4643

■ ASSOCIATED CONTENT

Supporting Information

Enlarged portion of neutron diffraction pattern in Figure 3 and accompanying CIF files for $LiMnTiO_4$ slowly cooled and quenched from 900 and 950 °C. The Supporting Information is available free of charge on the ACS Publications website at DOI: 10.1021/ic502747p.

■ AUTHOR INFORMATION

Corresponding Author

*E-mail: siegbert.schmid@sydney.edu.au.

Present Address

[§]Canadian Light Source, Saskatoon, SK, S7N 2 V3, Canada, and Department of Chemistry, University of Saskatchewan, Saskatoon, SK, S7N 5C9, Canada.

Author Contributions

The manuscript was written through contributions of all authors. All authors have given approval to the final version of the manuscript.

Notes

The authors declare no competing financial interest.

■ ACKNOWLEDGMENTS

Some of this work was performed at the powder diffraction beamline of the Australian Synchrotron, and the authors thank Dr. Q. Gu for his assistance. XANES spectra were recorded at the Australian National Beamline Facility with the help of Dr. J. Aitken and funding from the Access to Major Research Facilities Program supported by the Commonwealth Government of Australia. The authors also thank Mr. A. Pavan for help with TGA measurements.

■ REFERENCES

(1) Tarascon, J. M.; Wang, E.; Shokoohi, F. K.; McKinnon, W. R.; Colson, S. *J. Electrochem. Soc.* **1991**, *138*, 2859−2864.

(2) Hunter, J. C. *J. Solid State Chem.* **1981**, *39*, 142−147.

(3) Goodenough, J. B.; Park, K. S. *J. Am. Chem. Soc.* **2013**, *135*, 1167−1176.

(4) Kim, J. H.; Myung, S. T.; Yoon, C. S.; Kang, S. G.; Sun, Y. K. *Chem. Mater.* **2004**, *16*, 906−914.

(5) Cabana, J.; Casas-Cabanas, M.; Omenya, F. O.; Chernova, N. A.; Zeng, D.; Whittingham, M. S.; Grey, C. P. *Chem. Mater.* **2012**, *24*, 2952−2964.

(6) Song, J.; Shin, D. W.; Lu, Y. H.; Amos, C. D.; Manthiram, A.; Goodenough, J. B. *Chem. Mater.* **2012**, *24*, 3101−3109.

(7) Lee, E. S.; Nam, K. W.; Hu, E. Y.; Manthiram, A. *Chem. Mater.* **2012**, *24*, 3610−3620.

(8) He, G. N.; Li, Y. X.; Li, J.; Yang, Y. *Electrochem. Solid St.* **2010**, *13*, A19−A21.

(9) Wang, S. H.; Yang, J.; Wu, X. B.; Li, Y. X.; Gong, Z. L.; Wen, W.; Lin, M.; Yang, J. H.; Yang, Y. *J. Power Sources* **2014**, *245*, 570−578.

(10) Chen, R.; Knapp, M.; Yavuz, M.; Heinzmann, R.; Wang, D.; Ren, S.; Trouillet, V.; Lebedkin, S.; Doyle, S.; Hahn, H.; Ehrenberg, H.; Indris, S. *J. Phys. Chem. C* **2014**, *118*, 12608−12616.

(11) Krutzsch, B.; Kemmler-Sack, S. *J. Less-Common Met.* **1986**, *124*, 111−123.

(12) Suzuki, S.; Tomita, M.; Okada, S.; Arai, H. *J. Phys. Chem. Solids* **1996**, *57*, 1851−1856.

(13) Petrov, K.; Rojas, R. A.; Alonso, P. J.; Amarilla, J. A.; Lazarraga, M. G.; Rojo, J. A. *Solid State Sci.* **2005**, *7*, 277−286.

(14) Krins, N.; Hatert, F.; Traina, K.; Dusoulier, L.; Molenberg, I.; Fagnard, J. F.; Vanderbemden, P.; Rulmont, A.; Cloots, R.; Vertruyen, B. *Solid State Ionics* **2006**, *177*, 1033−1040.

(15) Avdeev, G.; Amarilla, J. M.; Rojo, J. M.; Petrov, K.; Rojas, R. M. *J. Solid State Chem.* **2009**, *182*, 3226−3231.

(16) Arillo, M. A.; Lopez, M. L.; Pico, C.; Veiga, M. L. *Solid State Sci.* **2008**, *10*, 1612−1619.

(17) Arillo, M. A.; Lopez, M. L.; Pico, C.; Veiga, M. L.; Jimenez-Lopez, A.; Rodriguez-Castellon, E. *J. Alloys Compd.* **2001**, *317*, 160−163.

(18) Arillo, M. A.; Cuello, G.; Lopez, M. L.; Martin, P.; Pico, C.; Veiga, M. L. *Solid State Sci.* **2005**, *7*, 25−32.

(19) Murphy, D. T. Honours Thesis, The University of Sydney, Sydney, Australia, 2011.

(20) Rietveld, H. M. *J. Appl. Crystallogr.* **1969**, *2*, 65−&.

(21) Petříček, V.; Dušek, M.; Palatinus, L. *Jana 2006 The Crystallographic Computing System;* Institute of Physics: Praha, Czech Republic, 2006.

(22) Ravel, B.; Newville, M. *J. Synchrotron Radiat.* **2005**, *12*, 537−541.

(23) Fairley, N. CasaXPS, Casa Software, Ltd.: Teignmouth, Devon, U.K., 2012.

(24) Brown, I. D.; Altermatt, D. *Acta Crystallogr., Sect. B* **1985**, *41*, 244−247.

(25) Farges, F. *Phys. Rev. B*, **2005**, *71*.

(26) Yamamoto, T. *X-Ray Spectrom.* **2008**, *37*, 572−584.

(27) Ammundsen, B.; Jones, D. J.; Roziere, J.; Burns, G. R. *Chem. Mater.* **1996**, *8*, 2799−2808.

(28) Belli, M.; Scafati, A.; Bianconi, A.; Mobilio, S.; Palladino, L.; Reale, A.; Burattini, E. *Solid State Commun.* **1980**, *35*, 355−361.

(29) Grosvenor, A. P.; Greedan, J. E. *J. Phys. Chem. C* **2009**, *113*, 11366−11372.

(30) Gaultois, M. W.; Grosvenor, A. P. *J. Mater. Chem.* **2011**, *21*, 1829−1836.

(31) Vedrinskii, R. V.; Kraizman, V. L.; Novakovich, A. A.; Demekhin, P. V.; Urazhdin, S. V. *J. Phys.: Condens. Matter* **1998**, *10*, 9561−9580.

DOI: 10.1021/ic502747p
Inorg. Chem. 2015, 54, 4636−4643